NIPPON STEEL & SUMITOMO METAL TECHNICAL REPORT No. 120 DECEMBER 2018

Technical Report

UDC 669 . 14 - 156 : 539 . 4 . 014 . 11 : 681 . 3

Effect of Implicit Integration Scheme on Residual Stress Analysis of Quenching Considering Transformation Plasticity and Kinematic Hardening

Yusuke KAWARAGI* Kazuo OKAMURA
Manabu FUKUMOTO

Abstract

Thermo-elastoplastic analysis considering the phase transformation has been widely used to predict the residual stress and distortion that accompanies the heat treatment. In the heat treatment simulation, transformation plasticity should be treated implicitly as it is relevant to the current stress field. Furthermore, the complex mechanical response caused by temperature change and phase transformation often leads to stress reversals, which may require kinematic hardening models in the heat treatment simulation. However, few of the previous studies have considered both the fully-implicit formulation and kinematic hardening model in the thermo-elastoplastic analysis including transformation plasticity. In this paper, therefore, thermo-elastoplastic constitutive relations considering the transformation plasticity and kinematic hardening are formulated with the return mapping algorithm, and heat treatment simulations of the steel cylinder are performed based on the proposed formulation. The calculated residual stresses show good agreement with the XRD measurements, and the capability of the fully implicit stress integration with the kinematic hardening model is demonstrated.

1. Introduction

Quenching is the heat treatment process that hardens steel material members in consequence of forming the martensite structure by rapid cooling from the austenitizing temperature. Various machine parts requiring high strength are commonly strengthened by quenching; however, the quenching frequently causes undesired distortion and/or residual stress in the members due to the difference of the cooling rate between the surface and the inner part of members. In addition, the volume change caused by the phase transformation also causes undesired distortion. Since these problems cause dimensional errors and/or deterioration in the fatigue strength of products, studies on the mechanism of generation of the residual stress have been conducted, and the optimization of production processes has been attempted. To date, a number of studies[1–13] dealing with the finite element method considering the phase transformation have been reported, and general-purpose software for the heat treatment simulation[4–6] has been developed. We have constructed a heat treatment simulation code[7] independently by incorporating a computational facility for the phase transformation to Abaqus, a general-purpose finite element analysis software, and have applied the software to the simulation of heat treatment in a number of steel products.

The elastoplastic analysis step is divided into small time increments to simulate material nonlinearity, and in each time increment repetitive computation (iteration) is applied until the equilibrating solution between the internal force and the external force is obtained. In the computation of the stress increment corresponding to the strain increment at each integration point during the iteration, the return mapping algorithm[14] is mainly used in static analysis. The return mapping algorithm is a method which pulls back the elastically predicted trial stress to the yield surface by generating

* Materials Reliability Research Lab., Steel Research Laboratories
1-8 Fuso-cho, Amagasaki City, Hyogo Pref. 660-0891

plastic strain increments.

During the progress of the phase transformation due to heat treatment, a large plastic strain is generated even when a stress lower than the yield stress of the material is applied. Such phenomenon is termed transformation plasticity. As the said transformation plasticity strain can become equal to or larger than the thermal strain and/or the plastic strain, it affects greatly the prediction of the residual stress caused by heat treatment. The transformation plasticity strain is proportional to the applied stress, of which the coefficient of proportionality is termed the transformation plasticity coefficient. By using the experimentally measured transformation plasticity coefficient, the transformation plasticity strain is calculated, and by adding the transformation plasticity strain to the elastic strain and/or the plastic strain in the thermo-elastoplastic analysis, various types of analysis are conducted.[2–13)] When the transformation plasticity strain is not considered in the return mapping algorithm, as the stress value at the current time is not appropriately incorporated in the calculation of the transformation plasticity, the equilibrium of the stress at the current time is not guaranteed, and the deterioration of analysis accuracy is caused. There are few detailed reports regarding the formulation of the return mapping algorithm that incorporates the transformation plastic strain calculated by using the abovementioned transformation plasticity coefficient.

Furthermore, in the inside of the material undergoing heat treatment, the cooling rate varies region by region, and the phase transformation and/or the generation of strain are heterogeneously developed. Therefore, the stress in the member varies complicatedly, causing the reversal between tension stress and compressive stress. Such reversal can take place as frequently as multiple times.[15)] Accordingly, by applying the kinematic hardening model to the heat treatment simulation, improvement of accuracy is expected in the residual stress prediction. In the past several studies, the kinematic hardening model was used for the analysis of the welding and quenching behavior.[1, 13)]

Regarding the heat treatment simulation, there are several studies that deal with the implicit solution incorporated with transformation plasticity,[10, 11)] or verify the effect of the kinematic hardening model. However, there have been no reports that deal with these theories simultaneously or study in detail the influence thereof on the analysis accuracy.

This study introduced the formulation of the return mapping algorithm of the elastoplastic constitutive relation incorporated with the transformation plasticity and the kinematic hardening model, and the prediction accuracy of the residual stress is inspected by conducting a quenching simulation of a steel cylinder. The influence of the implicit integration scheme on analysis accuracy is inspected by comparing the analysis results of the implicit and explicit calculation of transformation plasticity in the stress integration, and the hardening models are also inspected by comparing the quenching analysis results of the isotropic hardening model and the kinematic hardening model with the residual stress measured by X-ray diffraction.

2. Analysis Program

2.1 Calculation of transformation plasticity

In the heat treatment simulation, the strain attributed to the phase transformation needs to be considered in addition to the elastic strain, plastic strain, and the thermal strain used in the elastoplastic analysis,. The total strain increment $\Delta\boldsymbol{\varepsilon}$ in a time increment Δt when the phase transformation in the small deformation is considered is expressed by the following formula.

$$\Delta\boldsymbol{\varepsilon} = \Delta\boldsymbol{\varepsilon}_e + \Delta\boldsymbol{\varepsilon}_p + \Delta\boldsymbol{\varepsilon}_v + \Delta\boldsymbol{\varepsilon}_{TP} \tag{1}$$

Where, $\Delta\boldsymbol{\varepsilon}_e$: elastic strain increment, $\Delta\boldsymbol{\varepsilon}_p$: plastic strain increment, $\Delta\boldsymbol{\varepsilon}_v$: thermal and transformation strain increment, $\Delta\boldsymbol{\varepsilon}_{TP}$: transformation plasticity strain increment. $\Delta\boldsymbol{\varepsilon}_v$ is the strain increment attributed to the isotropic volume change caused by the changes in temperature and the metallic microstructure which can be calculated from the temperature T and the volume fraction ξ_I of the phase I as follows.[8)]

$$\Delta\boldsymbol{\varepsilon}_v = \frac{1}{3}\left(\frac{\sum_I {}^n\xi_I \rho_I\left({}^nT\right)}{\sum_I {}^{n+1}\xi_I \rho_I\left({}^{n+1}T\right)} - 1 \right) \tag{2}$$

Where the subscripts n and n+1 denote the values at the time of ${}^nt$ and the time of ${}^{n+1}t = t + \Delta t$. $\rho_I(T)$ is the density of the phase I at the temperature of T which is calculated from the prediction formula proposed by Miettinen[16)] that is based on the chemical compositions.

Regarding the transformation plasticity strain $\Delta\boldsymbol{\varepsilon}_{TP}$, Denis et al.[2)] proposed the following formula assuming that the transformation plasticity $\Delta\boldsymbol{\varepsilon}_{TP}$ depends on the volume fraction ξ of the formed phase and is proportional to the stress.

$$d\boldsymbol{\varepsilon}_{TP} = 3K\left(1-\xi\right) d\xi \mathbf{S} \tag{3}$$

Where $\mathbf{S}$ is the deviatoric stress and K is the transformation plasticity coefficient. In this study, the following formula, the extended formula of Formula (3) that meets the case with multiple phase transformation, was used.

$$\Delta\boldsymbol{\varepsilon}_{TP} = \sum_I 3K_I\left(1-\sum_J \xi_J\right)\Delta\xi_I \mathbf{S} \tag{4}$$

Where K_I is the transformation plasticity coefficient of the phase I. Since the transformation plasticity strain increment is proportional to the value of the deviatoric stress, the value of the stress at the current time is necessary for the calculation of the transformation plasticity strain increment.

When calculating the transformation plasticity strain increment explicitly, the stress increment and the plastic strain increment are implicitly calculated by the return mapping algorithm of the elastoplastic constitutive relation without considering the phase transformation after the transformation strain increment and the transformation plasticity strain increment are subtracted from the total strain increment as external force terms such as the thermal strain increment. Namely, the transformation plasticity strain increment is calculated by using not the stress of ${}^{n+1}\boldsymbol{\sigma}$ at the current time of ${}^{n+1}t$ but the stress of ${}^n\boldsymbol{\sigma}$ at the previous time of ${}^nt$. Therefore, the equilibrium of stress at the current time of ${}^{n+1}t$ is not guaranteed, and an error is generated against the correct solution. Deterioration of accuracy due to the error is unavoidable. As **Fig. 1** shows, the error of ${}^{n+1}\boldsymbol{\sigma}$ at the time of ${}^{n+1}t$ can be reduced by making the time increment Δt smaller. However, in the case that the time increment Δt is reduced, the number of increments, namely the number of computations, increases and the analysis time increases.

Then, by executing the return mapping algorithm that considers the transformation plasticity, the analysis accuracy was improved by not calculating the transformation strain increment explicitly but by calculating the transformation plasticity strain increment together with the stress increment and the plastic strain increment implicitly. To execute this analysis, the formulation of the return mapping algorithm employing the elastoplastic constitutive relation considering the transformation plasticity is required.

2.2 Calculation of phase transformation

In the heat treatment simulation, the calculation of the change in

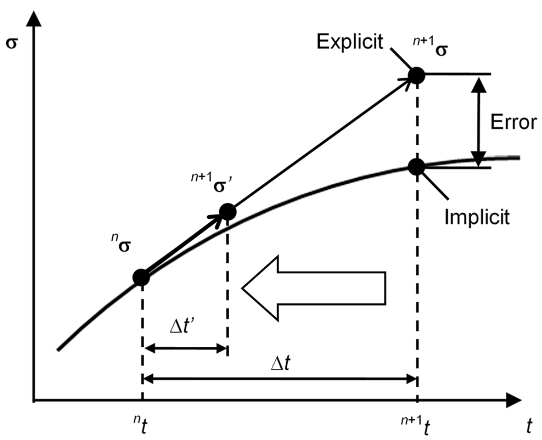

Fig. 1 Schematic diagram of analysis error

the phase fraction is required. Although the prediction of the phase transformation at an arbitrary temperature and an arbitrary time is possible by using the TTT curve of the subject steel, it is difficult to prepare the TTT curves for all steel types. Kirkaldy et al.[17] proposed a prediction formula for the transformation of steel for any chemical compositions. In this study, the modified form of the formula of Kirkaldy et al. proposed by Li et al.[18] is used, which is expressed as the following in the form of the isothermal transformation rate.

$$\frac{d\xi_I}{dt} = \frac{2^{k_I G_A}(T_I - T)^m \exp(-Q/RT)}{F_I(\mathrm{C,Mn,Si,Ni,Cr,Mo})}\,\xi_I^{0.4(1-\xi_I)}\,(1-\xi_I)^{0.4\xi_I} \quad (5)$$

Where, F_I: function of weight percent concentration of alloying elements of C, Si, Mn, Cr, Ni, Mo, k_I: constant which is determined by fitting to a number of publicized TTT data, Q: activation energy of diffusion transformation, G_A: austenite grain size number, R: gas constant, and m is a constant. T_I: transformation temperature which is the Ae3 temperature for ferrite, Ae1 temperature for pearlite, and Bs temperature for bainite. The prediction formula for the transformation upper limit temperature based on chemical compositions[18, 19] has been proposed. Assuming that the temperature is constant during a minimal time, the phase fraction in continuous cooling is calculated by integrating Formula (5). In the case of martensite with diffusionless transformation, the change in the phase fraction progresses depending on the temperature, regardless of time. Koistinen et al.[20] proposed the following regression formula based on the experimental data to estimate the martensite phase fraction, and this formula was used in this study.

$$\xi_M = 1-\exp\{-0.011(\mathrm{Ms}-T)\} \quad (6)$$

Where Ms is the martensite start temperature and a prediction formula based on chemical compositions[19] is used therefor.

2.3 Hardening model

In the cooling process of quenching, the cooling rate varies region by region in the inside of the material undergoing heat treatment, and the phase transformation and/or the strain are heterogeneously developed. Therefore, the stress in members varies complicatedly, causing the reversal between tensile stress and compressive stress multiple times. In the metallic material subject to repetitive loads, a model of kinematic hardening is used as the hardening model to express the elastoplastic behavior such as the Bauschinger effect, which the isotropic hardening model is unable to express. Then, the prediction accuracy of the residual stress caused by quenching is expected to be improved by introducing the kinematic hardening model to the heat treatment simulation. Then, in this study, in formulating the return mapping algorithm, the use of the kinematic hardening model was realized by employing the elastoplastic constitutive relation incorporated with the kinematic hardening model.

von Mises yield criterion that is generally used for metallic materials was used, and the mixed hardening model consisting of the isotropic hardening model and the kinematic hardening model was used. In the case that the kinematic hardening model is considered, von Mises yield function is expressed by the following formula.

$$f = \bar{\sigma} - Y = \sqrt{\frac{3}{2}(\mathbf{S}-\boldsymbol{\alpha}'):(\mathbf{S}-\boldsymbol{\alpha}')} - Y = 0 \quad (7)$$

Where, $\bar{\sigma}$: equivalent stress, Y: yield stress, and $\boldsymbol{\alpha}'$: deviatoric back stress.

The back stress is the variable that expresses the shift of the yield surface in the stress space. The model of Armstrong-Fredrick[21] is employed as the evolved model of the back stress, which is defined as the sum of the pure linear kinematic hardening term and the relaxation term of nonlinearity. By adding the nonlinear term, the stress-strain diagram can be expressed with high accuracy which the bilinear approximation is unable to express by fitting. The back stress $\boldsymbol{\alpha}'$ is expressed by the superimpositions of the components $\boldsymbol{\alpha}'_i$ of the back stress, and expressed as the following.

$$\boldsymbol{\alpha}' = \sum_i \boldsymbol{\alpha}'_i \quad (8)$$

$$^{n+1}\boldsymbol{\alpha}'_i = {}^{n}\boldsymbol{\alpha}'_i + c_i\Delta\boldsymbol{\varepsilon}_p - b_i\Delta p\,^{n+1}\boldsymbol{\alpha}'_i \quad (9)$$

Where, c_i, b_i: material constant, and Δp: equivalent plastic strain increment defined as Formula (10) below.

$$\Delta p = \sqrt{\frac{2}{3}\Delta\boldsymbol{\varepsilon}_p : \Delta\boldsymbol{\varepsilon}_p} \quad (10)$$

2.4 Formulation of return mapping algorithm

The formulation of the elastoplastic constitutive relation incorporating the transformation plasticity and the kinematic hardening model is shown below. The stress $^{n}\boldsymbol{\sigma}$ at the time of ^{n}t is assumed to be known, and the stress $^{n+1}\boldsymbol{\sigma}$ at the time of ^{n+1}t is expressed by the following formula.

$$\begin{aligned}
^{n+1}\boldsymbol{\sigma} &= {}^{n+1}\mathbf{C} : {}^{n+1}\boldsymbol{\varepsilon}_e \\
&= ({}^{n}\mathbf{C}+\Delta\mathbf{C}) : ({}^{n}\boldsymbol{\varepsilon}_e+\Delta\boldsymbol{\varepsilon}_e) \\
&= {}^{n}\mathbf{C} : {}^{n}\boldsymbol{\varepsilon}_e + \Delta\mathbf{C} : {}^{n}\boldsymbol{\varepsilon}_e + ({}^{n}\mathbf{C}+\Delta\mathbf{C}) : \Delta\boldsymbol{\varepsilon}_e \\
&= {}^{n}\boldsymbol{\sigma} + \Delta\mathbf{C} : {}^{n}\boldsymbol{\varepsilon}_e + {}^{n+1}\mathbf{C} : (\Delta\boldsymbol{\varepsilon}-\Delta\boldsymbol{\varepsilon}_v-\Delta\boldsymbol{\varepsilon}_p-\Delta\boldsymbol{\varepsilon}_{TP})
\end{aligned} \quad (11)$$

Where, $\mathbf{C}$: elastic coefficient tensor, and $\Delta\mathbf{C}$: increment of $\mathbf{C}$ due to change in temperature

In the case that there is no dependency of transformation on stress as in Formulae (5) and (6), as the thermal and transformation strain increment does not depend on the stress, and does not influence the return mapping algorithm, the strain increment of the total strain increment subtracted with $\Delta\boldsymbol{\varepsilon}_e$, $\Delta\boldsymbol{\varepsilon}_p$ and $\Delta\boldsymbol{\varepsilon}_{TP}$ is used, which is outlined as follows.

$$\Delta\boldsymbol{\varepsilon}_M = \Delta\boldsymbol{\varepsilon} - \Delta\boldsymbol{\varepsilon}_v \quad (12)$$

When all the strain increment is assumed as elastic strain, the stress is termed as the elastic predictor, which is expressed by the following formula.

$$\boldsymbol{\sigma}^{(T)} = {}^{n}\boldsymbol{\sigma} + \Delta\mathbf{C} : {}^{n}\boldsymbol{\varepsilon}_e + {}^{n+1}\mathbf{C} : \Delta\boldsymbol{\varepsilon}_M \quad (13)$$

Formula (11) is expressed as follows using the elastic predictor.

$$^{n+1}\boldsymbol{\sigma} = \boldsymbol{\sigma}^{(T)} - {}^{n+1}\mathbf{C} : (\Delta\boldsymbol{\varepsilon}_p + \Delta\boldsymbol{\varepsilon}_{TP}) \quad (14)$$

Based on the flow rule, the plasticity strain increment $\Delta\boldsymbol{\varepsilon}_p$ is expressed as follows.

$$\Delta \boldsymbol{\varepsilon}_p = \Delta p \frac{\partial f}{\partial \boldsymbol{\sigma}} = \frac{3\Delta p}{2\,{}^{n+1}\bar{\sigma}} \left({}^{n+1}\mathbf{S} - {}^{n+1}\boldsymbol{\alpha}' \right) \tag{15}$$

The parts not dependent on the stress in Formula (4) do not change during the execution of the return mapping algorithm, and are defined as Δh.

$$\Delta h = \sum_I 3K_I \left(1 - \sum_J \xi_J\right) \Delta \xi_I \tag{16}$$

Formula (4) is expressed as follows using Δh.

$$\Delta \boldsymbol{\varepsilon}_{TP} = \Delta h\, {}^{n+1}\mathbf{S} \tag{17}$$

By inserting Formulae (17) and (15) into Formula (14), removing the deviators from both sides, and using the conditions of Formula (7), Formula (14) becomes the following.

$$\Delta p \left(\frac{3\,{}^{n+1}G}{1+2\,{}^{n+1}G\Delta h} + \frac{3}{2} \sum_i \frac{c_i}{1+b_i \Delta p} \right) = \frac{\bar{\theta}}{1+2\,{}^{n+1}G\Delta h} - {}^{n+1}Y \tag{18}$$

Where $\bar{\theta}$ and $\boldsymbol{\theta}$ are expressed as follows.

$$\bar{\theta} = \sqrt{\frac{3}{2} \boldsymbol{\theta} : \boldsymbol{\theta}} \tag{19}$$

$$\boldsymbol{\theta} = \mathbf{S}^{(T)} - \left(1 + 2\,{}^{n+1} G \Delta h\right) \sum_i \frac{{}^{n}\boldsymbol{\alpha}'_i}{1+b_i \Delta p} \tag{20}$$

Where, $\mathbf{S}^{(T)}$: deviator of elastic predictor $\boldsymbol{\sigma}^{(T)}$ and G: shear modulus

By solving Equation (18), Δp is obtained. Since Equation (18) is a nonlinear equation with respect to Δp, it is computed numerically by the Newton-Raphson method to obtain the solution.

With the determination of the equivalent plastic strain increment, the stress and the respective strains at the time of ${}^{n+1}t$ are renewed as follows.

$${}^{n+1}\boldsymbol{\sigma} = {}^{n+1}\mathbf{S} + \frac{1}{3} \operatorname{tr}\left(\boldsymbol{\sigma}^{(T)}\right)\mathbf{I} = \boldsymbol{\theta} \frac{{}^{n+1}Y}{\bar{\theta}} + {}^{n+1}\boldsymbol{\alpha}' + \frac{1}{3} \operatorname{tr}\left(\boldsymbol{\sigma}^{(T)}\right)\mathbf{I} \tag{21}$$

$${}^{n+1}\boldsymbol{\alpha}' = \sum_i \frac{{}^{n}\boldsymbol{\alpha}'_i}{1+b_i \Delta p} + \frac{3}{2} \sum_i \frac{c_i}{1+b_i \Delta p} \Delta p \frac{\boldsymbol{\theta}}{\bar{\theta}} \tag{22}$$

$${}^{n+1}\boldsymbol{\varepsilon}_p = {}^{n}\boldsymbol{\varepsilon}_p + \frac{3}{2} \Delta p \frac{\boldsymbol{\theta}}{\bar{\theta}} \tag{23}$$

$${}^{n+1}\boldsymbol{\varepsilon}_{TP} = {}^{n}\boldsymbol{\varepsilon}_{TP} + \Delta h\, {}^{n+1}\mathbf{S} \tag{24}$$

$${}^{n+1}\boldsymbol{\varepsilon}_e = {}^{n}\boldsymbol{\varepsilon}_e + \Delta \boldsymbol{\varepsilon}_M - \frac{3}{2} \Delta p \frac{\boldsymbol{\theta}}{\bar{\theta}} - \Delta h\, {}^{n+1}\mathbf{S} \tag{25}$$

Where $\mathbf{I}$ is the identity tensor of the 2nd order. In the case that the plastic strain is not produced and only the transformation plastic strain is produced, the return mapping algorithm is not executed and the respective stress and the respective strain are renewed by inputting $\Delta p = 0$ to Formulae (21)–(25) instead.

In the elastoplastic analysis, when the equilibrium solution of the model is found, the calculation of the consistent tangent modulus that expresses the relation between the stress increment and the strain increment is necessary. The consistent tangent modulus $\mathbf{C}^{\mathrm{ep}}$ incorporating transformation plasticity is expressed by the formula below. The derivation process is omitted.

$$\mathbf{C}^{\mathrm{ep}} = \mathbf{C}' - \left[3G' - \frac{ \dfrac{3\,{}^{n+1}G}{1+2\,{}^{n+1}G\Delta h} \left\{ {}^{n+1}H' + \dfrac{3}{2} \sum_i \dfrac{c_i}{(1+b_i \Delta p)^2} \right\} - 3G' \left\{ \dfrac{3}{2} \sum_i \dfrac{b_i\, {}^{n}\boldsymbol{\alpha}'_i}{(1+b_i \Delta p)^2} \right\} : \dfrac{\boldsymbol{\theta}}{\bar{\theta}} }{ \dfrac{3\,{}^{n+1}G}{1+2\,{}^{n+1}G\Delta h} + \dfrac{3}{2} \sum_i \dfrac{c_i}{(1+b_i \Delta p)^2} + {}^{n+1}H' - \left\{ \dfrac{3}{2} \sum_i \dfrac{b_i\, {}^{n}\boldsymbol{\alpha}'_i}{(1+b_i \Delta p)^2} \right\} : \dfrac{\boldsymbol{\theta}}{\bar{\theta}} } \right] \frac{\boldsymbol{\theta}}{\bar{\theta}} \otimes \frac{\boldsymbol{\theta}}{\bar{\theta}}$$

$$- \frac{ \dfrac{3\,{}^{n+1}G}{1+2\,{}^{n+1}G\Delta h} - 3G' }{ \left[\dfrac{3\,{}^{n+1}G}{1+2\,{}^{n+1}G\Delta h} + \dfrac{3}{2} \sum_i \dfrac{c_i}{(1+b_i \Delta p)^2} + {}^{n+1}H' - \left\{ \dfrac{3}{2} \sum_i \dfrac{b_i\, {}^{n}\boldsymbol{\alpha}'_i}{(1+b_i \Delta p)^2} \right\} : \dfrac{\boldsymbol{\theta}}{\bar{\theta}} \right] } \left\{ \sum_i \frac{b_i\, {}^{n}\boldsymbol{\alpha}'_i}{(1+b_i \Delta p)^2} \right\} \otimes \frac{\boldsymbol{\theta}}{\bar{\theta}} \tag{26}$$

$\mathbf{C}'$ and G' in Formula (26) are expressed as follows.

$$\mathbf{C}' = 2G' \overset{4}{\mathbf{I}} + \left(K - \frac{2}{3} G' \right) \mathbf{I} \otimes \mathbf{I} \tag{27}$$

$$G' = {}^{n+1}G \left({}^{n+1}Y + \frac{3}{2} \Delta p \sum_i \frac{c_i}{1+b_i \Delta p} \right) \frac{1}{\bar{\theta}} \tag{28}$$

Where, K: bulk modulus, $\overset{4}{\mathbf{I}}$: identity tensor of the 4th order, and H': work hardening coefficient expressed as $H' = \partial Y / \partial \Delta p$.

3. Verification and Validation of Analysis Accuracy

3.1 Validation of effect of stress integration

The calculation functions of the above phase transformation and the return mapping algorithm were incorporated into the user subroutine of Abaqus, and the quenching analysis was executed. By comparing the analysis results of the explicitly and implicitly executed calculations regarding the transformation plasticity, the analysis accuracy was inspected. For the sake of comparison, the maximum allowable temperature change in the increment $\Delta T_{\max}$ was varied. The value of the time increment is determined so that the temperature increment does not exceed the predetermined $\Delta T_{\max}$. Therefore, if the maximum allowable temperature change in the increment $\Delta T_{\max}$ is large, the time increment becomes large and the analysis result error also becomes large.

Figure 2 shows the two-dimensional axisymmetric model simulating a steel cylinder 18 mm in diameter and infinitely long in the axial direction. Axisymmetric quadrangular first-order elements numbering 74 nodal points and 36 elements are used. All elements are of a 0.25 × 0.25 mm square shape, and the distances between nodal points are equal. As the boundary conditions: the displacement in the radius direction of the nodal points on the center axis is fixed, the displacement of the nodal points on the bottom edge in the z-direction is fixed, and the model is constrained so that the displacement of each nodal point on the top edge is all equal in the z-direction (equivalent to the generalized plain strain condition). The steel model was heated uniformly from the initial temperature of 20°C to 930°C at a heating rate of 1°C/s, and its surface was cooled under the conditions of an ambient temperature of 20°C and the heat transfer coefficient of 4 000 W/m²K. Material data of SCr420 were used. The actually measured values of mechanical properties such

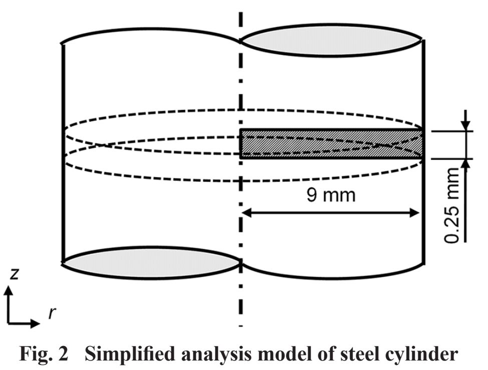

Fig. 2 Simplified analysis model of steel cylinder

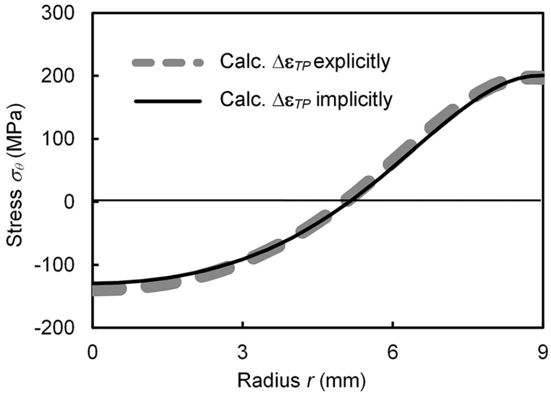

Fig. 3 Distribution of circumferential residual stress after quenching

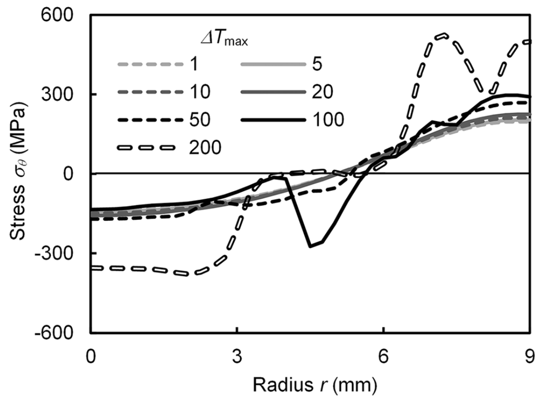

(a) Explicit calculation of transformation plasticity

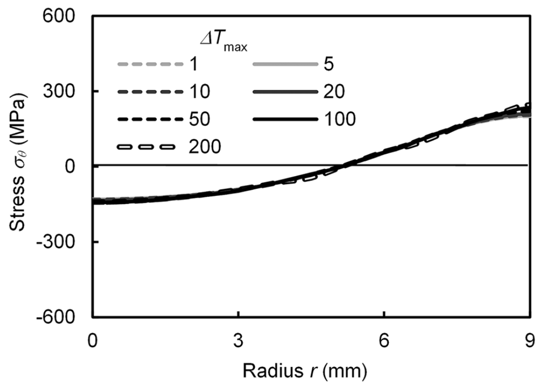

(b) Implicit calculation of transformation plasticity

Fig. 4 Distribution of circumferential residual stress varying ΔT_{max}

as Young's Modulus and the stress-strain curve were used. The thermal properties such as heat conductivity and specific heat were predicted and used, using Miettinen's formula[16] based on the chemical compositions of SCr420.

Figure 3 shows the distributions of the circumferential residual stress in the radial direction after the completion of quenching in the heat treatment simulation, obtained by the explicit and implicit calculations of the transformation plasticity. The maximum allowable temperature change in the increment ΔT_{max} is set at 1°C. The result indicates that the practically equal analysis results can be obtained from both calculations in the case that the time increment is sufficiently small.

Figure 4 shows the distributions in the radial direction of the circumferential residual stress after the completion of quenching in the heat treatment simulation, wherein the transformation plasticity was calculated and obtained explicitly (a) and implicitly (b), and the influence of the change in the maximum allowable temperature in the increment ΔT_{max} was examined. In the case that the transformation plasticity is calculated explicitly, the larger the time increment is, the larger the error becomes. In the case that ΔT_{max} exceeds 100°C, the realization of correct analysis becomes almost impossible. On the other hand, in the case that the transformation plasticity is calculated implicitly, even though the time increment is large, the error is small as compared with that of the explicit calculation, and the analysis of high accuracy can be executed. Since sufficient analysis accuracy is maintained even when the time increment is large, the analysis computation speed can be enhanced by increasing the time increment.

3.2 Validation of convergence rate

The validity of the consistent tangent modulus of Formula (26) was inspected by examining the convergence rate of the iteration. In the elastoplastic analysis, the consistent tangent modulus is used when calculating the correction amount of the displacement increment in the Newton-Raphson method, where the quadratic convergence rate is guaranteed when the consistent tangent modulus is correct. The analysis model of Section 3.1 was used. In order to inspect Formula (26) precisely, the kinematic hardening model was used for the hardening model, and the convergence of the increment in which both the plastic strain increment and the transformation plasticity strain increment occur was inspected. The parameters of the kinematic hardening model were obtained by fitting the model to the stress-strain curve of the uniaxial tensile test of the respective phase in the temperature range from 20°C to 900°C. Formula (26) is unsymmetrical, and the solver of the symmetrical matrix cannot be used, therefore, the computation cost becomes higher.

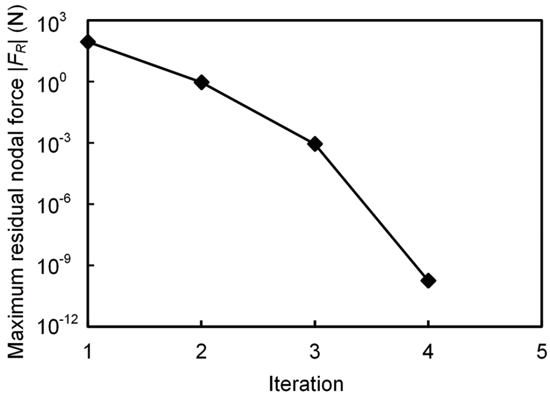

Fig. 5 Relationship between iteration and maximum residual nodal force

Figure 5 shows the relationship between the iteration and the maximum residual nodal force in the convergence computation of the equilibrium solution of the model. From Fig. 5, it was confirmed that the residual nodal force converges quadratically by using the consistent tangent modulus worked out in this study, and that the derivation of the consistent tangent modulus is valid.

4. Application to Quenching Analysis

4.1 Analysis method

In order to inspect the influence of the hardening model in the heat treatment simulation, the quenching analysis using only the isotropic hardening model as the hardening model, and the one using only the kinematic hardening model were conducted. The simulation results were compared with the XRD-measured residual stress obtained from the quenching test conducted from May, 2009 until March, 2012 by the quenching and its simulation study group of The Japan Society for Heat Treatment[22]. **Figure 6** shows the two-dimensional axisymmetric analysis model simulating a cylinder of 18 mm in diameter and 100 mm in length. The number of nodal point is 3096, the number of elements is 2944, and the minimum element size is 0.2 mm. As the boundary condition, the displacement in the radius direction of the nodal points on the center axis and the displacement in the *z*-direction of the nodal points in the center were fixed. After heating uniformly from the initial temperature of 20°C to 850°C at the heating rate of 1°C/s, its surface was water-cooled. The heat transfer coefficient was determined by means of inverse analysis based on the measured result obtained from an actual quenching test[22]. The material data of SCr430 were used.

4.2 Analysis result and examination

Figure 7 shows the history of the circumferential stress and the plastic strain at the surface of the center part of the cylinder. Figure 7 confirms that in either case of the isotropic hardening model or of the kinematic hardening model, tensile stress and tensile plastic strain are produced immediately after the start of cooling. After that, when the stress is reversed toward the compression direction, a difference in the elastoplastic behavior is observed between the kinematic deformation model and the isotropic deformation model. Differently from the plastic strain in the kinetic hardening model moving in the direction of compression, in the isotropic hardening model, the plastic strain hardly changes. Therefore, the difference in the stress is considered to have emerged. As the plastic strain has greatly changed after the stress reversal, it was confirmed that the yield surface has shifted and the yield stress has decreased by applying the kinematic hardening model.

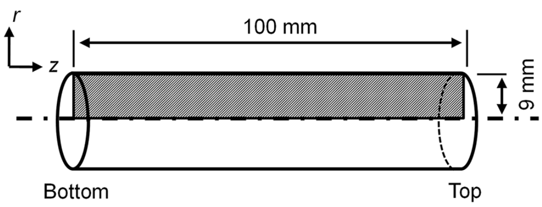

Fig. 6 Analysis model of steel cylinder

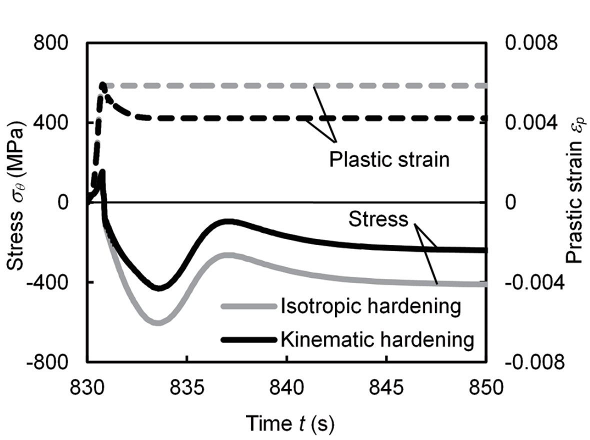

Fig. 7 History of circumferential stress and plastic strain during quenching

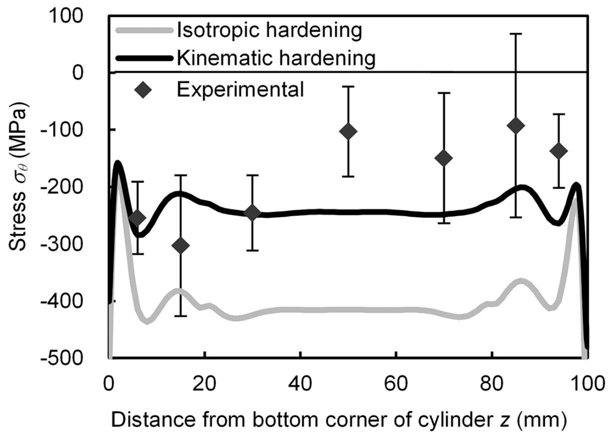

Fig. 8 Distribution of residual stress at surface after quenching

Figure 8 shows the distribution of the residual stress at the surface after quenching in the axial direction of the cylinder when the isotropic hardening model and the kinematic hardening model were applied. The tensile residual stress with the application of the kinematic hardening model is smaller than the one with the application of the isotropic hardening model, and is closer to the values measured by X-ray diffraction. Therefore, it was shown that the prediction accuracy of the heat treatment residual stress is improved by applying the kinematic hardening model to the heat treatment simulation.

5. Conclusion

This study shows the formulation of the return mapping algorithm of the elastoplastic constitutive relation incorporating the transformation plasticity and the kinematic hardening model, and by conducting an analysis simulating the quenching test of a steel cylinder, the effect of the implicit calculation of the transformation plasticity on the improvement of the analysis accuracy was inspected, and the validity of the hardening model was verified by comparing the residual stress obtained by the quenching analysis with the result measured by X-ray diffraction.

As a result thereof, it was confirmed that the analysis accuracy can be improved greatly by calculating the transformation plasticity implicitly rather than explicitly. Furthermore, in the quenching where the reversal between the tensile stress and the compressive stress is observed, the residual stress closer to the experimental result was obtained by introducing the kinematic hardening model to the heat treatment simulation.

The heat treatment simulation program established in this study is applied to the problem-solving in the heat treatment of actual products. Concerning products such as gears and shafts for automobile use where the strain produced in quenching is problematic, this program has shown good results by elucidating the mechanism of the generation of heat treatment distortion, and by proposing the strain-reducing quenching method.

This article was introduced in “Materials”[23], the Journal of The Society of Materials Science, Japan, and its copyright belongs to the Society.

References

1) Inoue, T. et al.: Ingenieur-Archiv. 50, 315 (1981)
2) Denis, S. et al.: Mech. Phys. Solids. 1 (10), 805 (1985)

3) Okamura, K. et al.: 32nd Japan Congress on Materials Research. 1989, p. 323
4) Inoue, T. et al.: Proceedings of the first International Conference on Quenching and Control of Distortion. 1992, p. 205
5) Nagasaka, Y.: Metal. Trans. 24A, 795 (1993)
6) Arimoto, K. et al.: Proceedings 18th Heat Treating Conference. ASM International, 1998, p. 639
7) Fukumoto, M. et al.: J. Soc. Mater. Sci. 50 (6), 598 (2001)
8) Okamura, K.: J. Soc. Mater. Sci. 55 (5), 529 (2006)
9) Simsir, C. et al.: J. Mater. Process. Tech. 207, 211 (2008)
10) Mahnken, R. et al.: Int. J. Plast. 25, 183 (2009)
11) Lee, M. G. et al.: Int. J. Plast. 25, 1726 (2009)
12) Deng, D. et al.: Comp. Mater. Sci. 78, 55 (2013)
13) Hamelin, C. J. et al.: Acta Mater. 75, 1 (2014)
14) Ortiz, M. et al.: Int. J. Numer. Meth. Eng. 21, 1561 (1985)
15) Sinha, A. K. et al.: ASM Handbook. 4, 1991, p. 601
16) Miettinen, J.: Metall. Mater. Trans. 28B, 281 (1997)
17) Kirkaldy, J. S. et al.: AIME. 125 (1983)
18) Li, M. V. et al.: Metall. Mater. Trans. 29B, 661 (1998)
19) Kunitake, T.: J. Jpn. Soc. Heat Treat. 41, 164 (2000)
20) Koistinen, D. P. et al.: Acta Metall. 7, 59 (1959)
21) Armstrong, P. J. et al.: Metall. Mater. Trans. Central Electricity Board Report RD/B/N, 731, (1966)
22) Activity Report of Quenching and Its Simulation Study Group: JSHT, 2012
23) Kawaragi, Y. et al.: J. Soc. Mater. Sci. Jpn. 64, 258 (2015)

Yusuke KAWARAGI
Materials Reliability Research Lab.
Steel Research Laboratories
1-8 Fuso-cho, Amagasaki City, Hyogo Pref. 660-0891

Manabu FUKUMOTO
Senior Researcher
Research Administration Dept.
R & D Planning Div.

Kazuo OKAMURA
Fellow, Doctor (Energy Science)
R & D Laboratories